Nano Research

ISSN 1998-0124 CN 11-5974/O4
https://doi.org/10.1007/s12274-020-3022-3

Research Article

Two-dimensional MX Dirac materials and quantum spin Hall insulators with tunable electronic and topological properties

Yan-Fang Zhang[1,2,§], Jinbo Pan[2,†,§], Huta Banjade[2], Jie Yu[2], Hsin Lin[3], Arun Bansil[4], Shixuan Du[1] (✉), and Qimin Yan[2] (✉)

[1] *Institute of Physics & University of Chinese Academy of Sciences, Chinese Academy of Sciences, Beijing 100190, China*
[2] *Department of Physics, Temple University, Philadelphia, PA 19122, USA*
[3] *Institute of Physics, "Academia Sinica", Taipei 11529*
[4] *Physics Department, Northeastern University, Boston, MA 02115, USA*
[†] *Present address: Institute of Physics & University of Chinese Academy of Sciences, Chinese Academy of Sciences, Beijing 100190, China*
[§] *Yan-Fang Zhang and Jinbo Pan contributed equally to this work.*

Received: 12 June 2020 / **Revised:** 28 July 2020 / **Accepted:** 29 July 2020

ABSTRACT

We propose a novel class of two-dimensional (2D) Dirac materials in the MX family (M = Be, Mg, Zn and Cd, X = Cl, Br and I), which exhibit graphene-like band structures with linearly-dispersing Dirac-cone states over large energy scales (0.8–1.8 eV) and ultra-high Fermi velocities comparable to graphene. Spin-orbit coupling opens sizable topological band gaps so that these compounds can be effectively classified as quantum spin Hall insulators. The electronic and topological properties are found to be highly tunable and amenable to modulation via anion-layer substitution and vertical electric field. Electronic structures of several members of the family are shown to host a Van-Hove singularity (VHS) close to the energy of the Dirac node. The enhanced density-of-states associated with these VHSs could provide a mechanism for inducing topological superconductivity. The presence of sizable band gaps, ultra-high carrier mobilities, and small effective masses makes the MX family promising for electronics and spintronics applications.

KEYWORDS

two-dimensional, Dirac materials, density functional theory, topological properties

1 Introduction

The presence of Dirac-cone structures and singularities in the electronic energy spectra of functional materials can endow them with unique properties and promising prospects for both fundamental research and applications [1]. The discovery of graphene, a monolayer honeycomb structure composed of carbon atoms [2], has spurred intense interest in the exotic physics associated with massless fermions, half-integer [3, 4]/fractional [5, 6]/fractal [7–9] quantum Hall effects (QHE), quantum spin Hall effect (QSH) [10] and other novel phenomena and properties [11, 12]. Within the vast space of inorganic two-dimensional (2D) compounds [13–17], graphene [3, 4, 18], silicene and germanene [19], graphynes [20, 21], and other related systems have been predicted to be Dirac materials [1, 22]. Dirac cones have been unambiguously confirmed by experiment in graphene. Experimental identification of Dirac-cone structure in silicene and germanene is still controversial [23–25], where appropriate substrates are needed to preserve the coherence of the Dirac cones. Experimental progress toward identifying Dirac states in more complex 2D structures, such as the graphynes, is still in its infancy [26]. It is therefore highly desirable to continue the search for novel 2D Dirac systems.

Considering the various requirements associated with crystal symmetries and chemical orbital interactions, it is a challenging task to search for novel 2D systems hosting Dirac cones close to the Fermi energy. Within the framework of tight-binding approximations, the occurrence of Dirac cone is driven by the presence of appropriate combinations of hopping energies [27, 28], which are controlled by details of the atomic geometries and the types of 2D crystal lattices involved in a given material. A simple analysis shows that a hexagonal cell is the most favorable host for Dirac cones [28]. Notably, both the time-reversal and spatial-inversion symmetries, which are present in most materials, and provide effective constraints on the Hamiltonian and play a key role in the generation of Dirac-cone structures [1]. Common features in the atomic structures include an even number of atoms in the unit cell and their bipartite nature of the lattice. These constraints can be used as descriptors for guiding the search for novel 2D Dirac compounds.

In this work, utilizing a hypothesis-based discovery process with our recently developed 2D materials electronic structure database (unpublished), we identify a novel class of 2D Dirac compounds with hexagonal lattices. First-principles computations based on density functional theory along with a related tight-binding analysis show that the MX monolayer materials family (M = Be, Mg, Zn and Cd, X = Cl, Br and I) hosts graphene-like band structures with Dirac cones located at the boundaries of the Brillouin zone. Based on atomic orbital

Address correspondence to Qimin Yan, qiminyan@temple.edu; Shixuan Du, sxdu@iphy.ac.cn

analysis, we discuss how Dirac cones emerge in this class of 2D systems with a charge-unbalanced chemical formula. When spin-orbit coupling (SOC) effects are included, these compounds yield time-reversal-invariant quantum spin Hall insulators. A subset of the MX family is found to host a Van-Hove singularity (VHS) with an enhanced density-of-states close in energy to the Dirac cones, which is often associated with unconventional superconductivity. This offers the possibility for the material to host topological superconductivity, such as the d+id chiral superconductivity or the odd-parity f-wave superconductivity [29, 30]. The topologically nontrivial electronic structure revealed here exhibits high tunability and it can be effectively modulated via anion substitution or vertical electric field, suggesting that this MX family would be of interest in developing materials platforms for nano-electronics applications.

2 Results and discussion

We initiated our discovery process from a materials dataset of ~ 880 compounds in our 2D electronic structure database. Initial structure search was guided by the hypothesis that the Dirac-cone electronic structure is favored in hexagonal lattices with additional symmetry constraints and crystal-system signatures. We chose bipartite systems with an even number of atoms in the unit cell as favorable factors for producing Dirac cone states in the electronic structure [1]. Only nonmagnetic compounds with inversion symmetry were considered. The candidates that passed through the initial screening were subjected to cation/anion substitutions to enlarge the chemical design space. In this way, our hypothesis-driven search yielded the novel class of MX (M = Be, Mg, Zn and Cd, X = Cl, Br and I) compounds with *P*3*m*1 plane-group to host the Dirac cone structures.

Monolayer MX compounds have an X–M–M–X sandwich structure forming a buckled honeycomb lattice with two sublattices (Fig. 1(a)). Taking the example of monolayer BeCl, we illustrate the interplay between its crystal structure and the appearance of Dirac-cone electronic structure. Each Be atom bonds with three Cl atoms and three Be atoms with Be–Be and Be–Cl bond lengths of 2.61 and 2.17 Å, respectively. Based on a Bader charge analysis, charge transfer from a Be atom to the neighboring Cl atoms is 0.93 |*e*|, which is consistent with the large electronegativity difference between Cl and Be (3.16 vs. 1.57 on the Pauling scale for Cl and Be, respectively) and indicates an ionic Be–Cl bonding character. Due to an unbalanced chemical formula, the cation-to-anion charge transfer leaves one electron on each Be atom, effectively forming a covalent hexagonal bonding network (Fig. 1(b)).

Band structure of BeCl (Fig. 1(c)) without SOC shows that two bands meet at the Fermi energy at the K point. The linear energy dispersion of the two bands in the energy range from −1.0 to 0.8 eV relative to the Fermi energy (inset of Fig. 1(c)) indicates that the charge carriers are graphene-like Dirac fermions. The energy dispersion can be described by $E = \hbar v_F k$, where v_F is the Fermi velocity and k is the wave vector. The calculated Fermi velocity in BeCl is 6.64×10^5 m/s for electrons and 4.76×10^5 m/s for holes, which are comparable to the velocities reported in 2D materials with high Fermi velocity [31–33]. No other band is present over the large energy range extending from −3.5 to 3.0 eV (relative to the Fermi energy), which is optimal for the detection of Dirac cone as well as for carrier modulation needed in applications. Figure 1(d) shows an overview of the Dirac-cone structures located at the six K points in the Brillouin zone. The band structure of BeCl/h-BN (Fig. S1 in the Electronic Supplementary Material (ESM)) clearly displays a preserved Dirac-cone band on the h-BN substrate, indicating the possibility of examining Dirac-cone related exotic phenomena using spectroscopic techniques.

The emergence of Dirac-cone electronic structure is universal in the MX compound family, which was constructed by substituting the cation (Mg, Zn, Cd) or anion atoms (Br, I) with other elements. All these monolayer structures were found to host similar Dirac-cone structures at the Fermi energy as well as ultra-high Fermi velocities, indicating that the Dirac-cone structure originates from the unique occupation of the outermost electronic orbitals in this family. The electronic and ground state properties of other MX members are given in Fig. S2(a) and Table S1 in the ESM.

With the inclusion of SOC (Fig. 1(e)), the Dirac cone in monolayer BeCl opens up a band gap of 12 meV, which is larger than that in graphene (0.8×10^{-3} meV) [34], but it is comparable to the predicted value in silicene (8.4 meV) and is

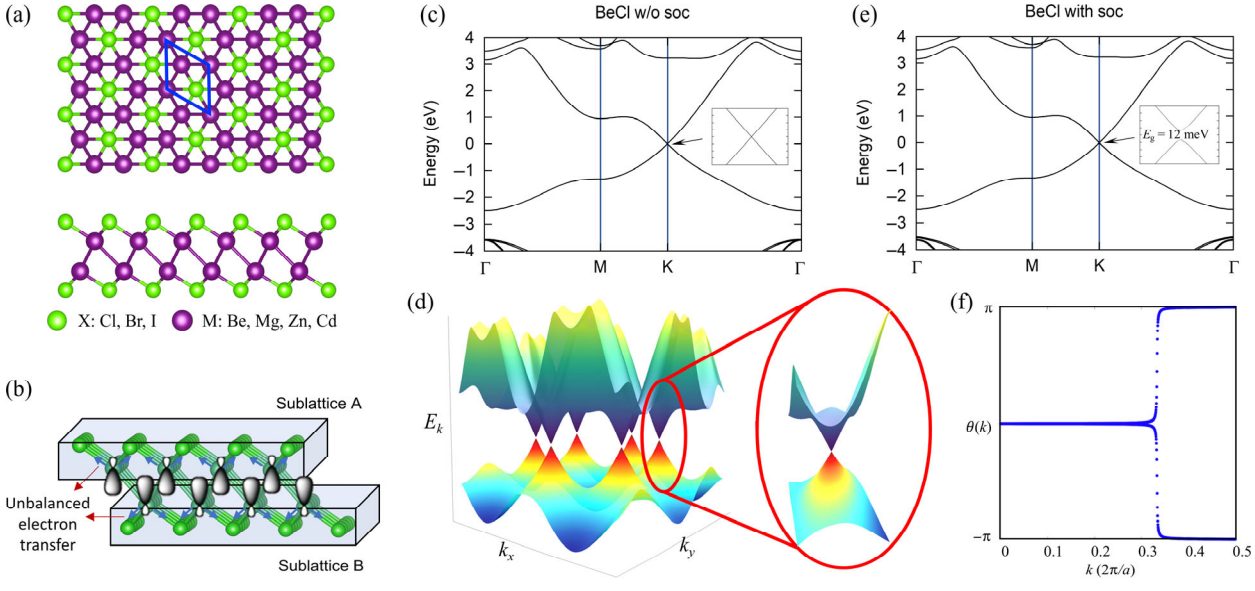

Figure 1 Geometric and electronic structure of MX. (a) Top and side views of the crystal structure of the MX (M = Be, Mg, Zn and Cd; X = Cl, Br and I) family of compounds. (b) A schematic of Dirac cone formation in MX compounds through unbalanced electron transfer and sidewise hybridized orbitals. (c) Band structure of BeCl without spin-orbit interaction. (d) A 3D view of the valence and conduction bands in the vicinity of the Dirac point. (e) Band structure of BeCl with spin-orbit interaction. (f) Wannier charge-center evolution in BeCl.

about half of that in germanene (23.6 meV) [35, 36]. The band gaps of other MX materials with the inclusion of SOC ranges from 4 to 178 meV. The results are summarized in Table S1 in the ESM. Next, we evaluate the topological property of BeCl by using the Wilson band, which is an open curve traversing the Brillouin zone (BZ) in the time-reversal invariant plane. Our calculations display an odd number of Wilson bands winding the BZ (Fig. 1(f)), which indicates that the Z_2 invariant equals 1. This class of MX 2D compounds thus realize the quantum-spin-Hall insulators state.

In the MX compound space, layered ScCl [37], ZrBr [38], and ZrCl [39] with the same atomic structure have been successfully synthesized. Electronic structures of ScCl, ZrBr, and ZrCl have been studied computationally [40]. 2D ScCl monolayer has been predicted to host intrinsic ferromagnetism [41]. The phonon dispersion was calculated to estimate its dynamical stability as summarized in Fig. S2(b) in the ESM. The absence of imaginary modes in the entire BZ indicates the dynamic stability of these monolayers. Molecular dynamic simulations were performed to evaluate the thermal stability. The result for MgCl, presented in Fig. S3 in the ESM, shows good thermal stability at room temperature. The calculated cohesive energy of BeCl (α-BeCl) is 3.15 eV/atom, comparable to another phase of BeCl (β-BeCl) monolayer (~ 3.27 eV/atom), which has been predicted as a semiconductor with a tunable band gap and good stability [42], but lower than bulk $BeCl_2$ (3.74 eV/atom). Since the lattice constant of α-BeCl is close to that of β-BeCl, being 3.14 and 3.26 Å, respectively, based on our calculations (it is 3.27 Å for β-BeCl from reference [43]), it is not clear that a selective growth of α-BeCl can be achieved by using different substrates. However, we note that even though this proposed phase is metastable, some of the other proposed compounds could possibly be fabricated via controlled growth techniques using different growth times and/or temperatures [43, 44].

We turn next to discuss how the Dirac-cone electronic structure emerges in the proposed MX compounds from the interplay of the frontier orbitals and lattice structure. The projected densities of states (Figs. 2(a) and 2(b)) clearly show that the dominant orbitals contributing close to the Dirac point are the s- and p_z- orbitals of Be atoms with an s–p hybridized nature. The partial charge density between −1 and 1 eV (relative to the Fermi energy) represents the dominant contribution from Be atoms (Fig. 2(c)). Furthermore, the Be charge is confined to the region between the two Be layers, which can be attributed to the contribution from the Be p_z orbitals. Dirac cones in the MX compounds thus originate through a novel combination of unbalanced chemical formula, orbital hybridization of group-II cations, and sidewise interactions between the two sublattices in a bipartite cation network. The s and p states in the cation atom form a set of sp^3 orbitals, through which three bonds are formed between the cation and three anions. Due to the unbalanced chemical formula, only one electron of the group-II cation is transferred to the three anion atoms through the σ bonds formed by the cation sp^3 orbitals and anion p orbitals. One electron remains in the sp^3-like orbital that points along the z direction toward the other sublattice. It is the sidewise overlapping of these sp^3 orbitals from the two sublattices that creates the bonding π and antibonding π^* states sandwiched between the two metal layers (Fig. 1(b)). The bonding π band is fully occupied by the remaining electrons, effectively placing the Fermi energy at the Dirac point. To further clarify this picture, we carried out a crystal-Hamiltonian-orbital-population (COHP) [45] analysis of the two states close to the Dirac point (Fig. S4 in the ESM). Metal-s/metal-p_z and metal-p_z/metal-p_z bonding interactions are observed immediately below the Dirac point, while antibonding interactions are presented above the Dirac point. These observations strongly support the novel mechanism we propose for the formation of Dirac cones in the MX family of 2D materials.

Further insight into the nature of the frontier orbitals can be obtained from the computed work functions (Fig. 2(d)), which are strongly correlated with the s orbitals of cation species (see detailed explanation in the ESM). By hosting a broad distribution of work functions, the MX family offers interesting opportunities for the design of heterojunction-based devices such as the tunneling transistors by taking advantage of the Dirac cone states. With the information of the frontier orbitals close to the Fermi energy in hand, the emergence of the Dirac cone in monolayer BeCl can be effectively understood within our effective tight-binding model [46, 47], which is described in detail in the ESM.

The unique band structures of MX compounds also offer a platform for exploring the interplay between topological physics

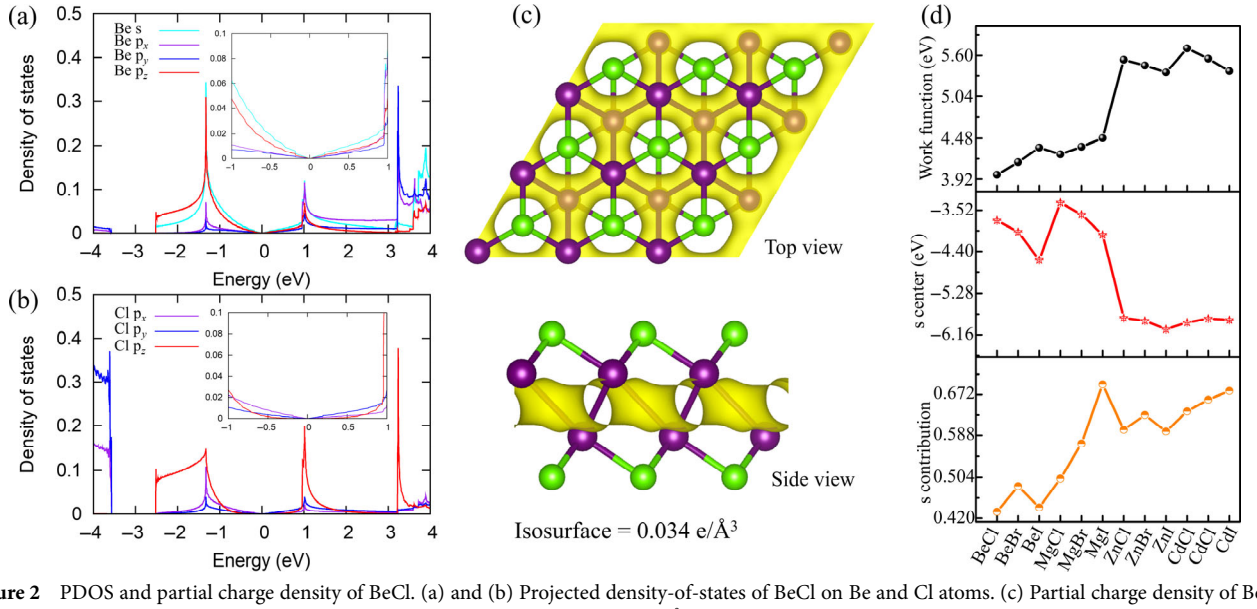

Figure 2 PDOS and partial charge density of BeCl. (a) and (b) Projected density-of-states of BeCl on Be and Cl atoms. (c) Partial charge density of BeCl from −1 to 1 eV relative to the Fermi energy, with an isosurface value of 0.034 e/Å^3. (d) Work functions, s-orbital centers, and s-orbital contributions in MX compounds.

and superconductivity. For example, the band structure of MgCl (Fig. 3(a)) hosts a VHS, which lies close in energy to the Dirac cone. Notably, other MX family members also exhibit the VHS in their electronic band structures (Fig. S2(a) in the ESM), although the VHSs in these other compounds lie farther away from the Fermi energy compared to the case of MgCl. The energy separation in MgCl between the VHS and the Dirac cone is 0.28 eV, which could be modulated by doping and electric field. Figure 3(b) shows the density of states (DOS) with a logarithmic singularity. This indicates the presence of a saddle-point where the massless Dirac cone meets with the pocket centered at M and presents a transition from an electron-like to a hole-like Fermi surface (Fig. 3(c)) when the chemical potential is raised. Position of a VHS in the reciprocal lattice space is presented in Fig. 3(d) as an example. It has been suggested that the enhanced DOS associated with VHSs could drive unconventional superconductivity. In the electron doped MgCl, there are six VHS points located between the M and K points, offering the possibility of odd-parity f-wave order. When considering the hole-doped case, there are 3 VHS points around −1 eV located at the M points. This is similar to the case of graphene and would favor chiral d+id superconductivity [29, 30]. The two aforementioned superconducting orders are desirable type of topological superconductivities.

Since the discovery of Dirac-cone structure in graphene, the introduction of a band gap while preserving high carrier mobility has proven to be a challenging task because even a moderate gap opening in graphene is accompanied with a large deterioration of carrier mobility. In contrast, in the monolayer MX compounds, the buckled honeycomb (metal) lattice is intercalated between the two layers of anion atoms, offering unique opportunities for modulating band structures. By inducing an electric potential difference between the atoms in different sublattices and breaking their equivalence, vertical electric field (Fig. 4(a)) is an effective approach for opening a band gap in the vicinity of the Fermi energy [48, 49]. Dependence of the calculated band gap in BeCl (with SOC) on the vertical electric field can be seen in Fig. 4(b). Similar to the case of graphene [50], the electric field gradually closes the band gap until it reaches zero at a critical point. An even larger electric field reopens the band gap and the system becomes a

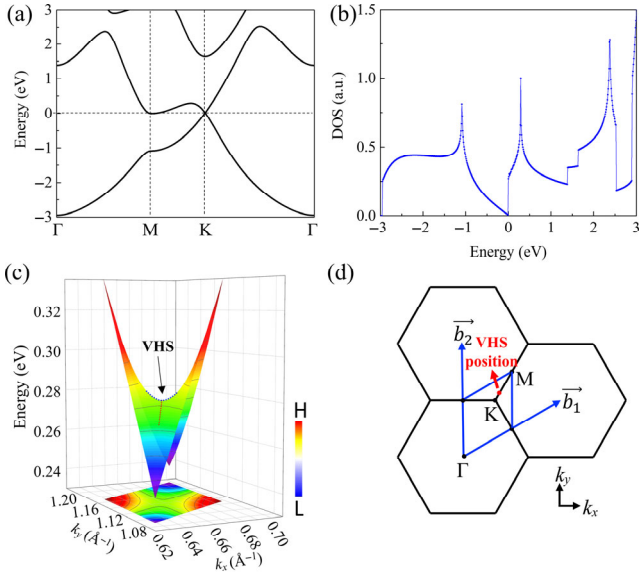

Figure 3 Electronic structure of MgCl. (a) and (b) Band structure and density-of-states of MgCl. (c) A 3D view and a contour plot of MgCl in the vicinity of the saddle point at $0.38b_1 + 0.38b_2$, where b_1 and b_2 are the reciprocal lattice vectors. (d) One of the VHS positions in the reciprocal.

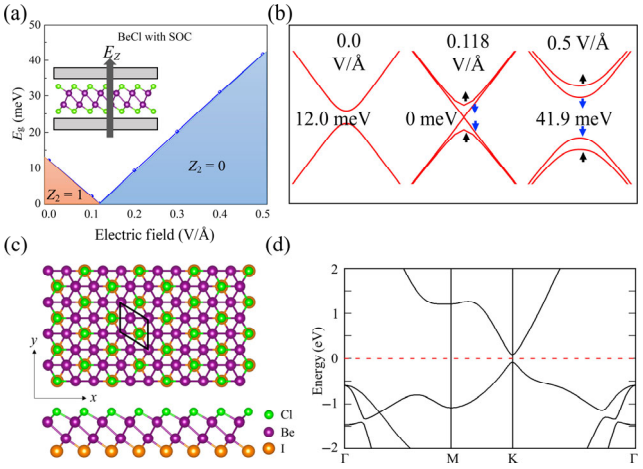

Figure 4 Band structure engineering of BeCl. (a) Schematic showing the application of a vertical electric field. (b) Band gap of BeCl as a function of the vertical electric field; band gaps are 12.0, 0 and 41.9 meV at 0.0, 0.118 and 0.5 V/Å, respectively. (c) Top and side views of Be_2ClI. The green, purple and orange balls represent Cl, Be and I atoms, respectively. (d) Band structure of Be_2ClI with a gap opening at the Fermi energy.

trivial insulator. By applying a 0.5 V/Å field, monolayer BeCl opens a band gap of ~ 41.9 meV, which is comparable to that predicted for germanene (~ 60 meV [48]). (Considering the underestimation of band gaps in calculations, the actual band gap is expected to be larger.)

As another example of band structure modulation, we consider a Be_2ClI structure obtained by substituting one layer of Cl atoms with I atoms (Fig. 4(c)), which in principle could be achieved using doping techniques [51, 52]. The optimized lattice constant is 3.47 Å, which as expected is larger than that of BeCl due to the larger atomic radius of I atoms. Band structure of the Be_2ClI (Fig. 4(d)) shows a sizable band gap (0.17 eV using the generalized-gradient approximation (GGA)-Perdew–Burke–Ernzerhof (PBE) functional and 0.22 eV using the HSE hybrid functional) at the K point, while the large dispersion of the conduction and valence bands is preserved. Note that this band gap is much larger than the predicted band gap in modulated graphene on h-BN, which is only tens of meV [53]. Moreover, we find electronic and valley polarization [54, 55] in Be_2ClI (Fig. S5 in the ESM), which would suggest its potential use in valleytronics. We estimated the carrier mobilities in Be_2ClI by applying a simple phonon-limited scattering model [56]; the related computational details and fitting curves are presented in Table S2, and Figs. S6 and S7 in the ESM. The computed carrier mobilities of Be_2ClI are on the order of 10^5 $cm^2/(V{\cdot}s)$, which are two orders of magnitude larger than those of single- and few-layer black phosphorus [57]. The sizable band gap combined with high carrier mobilities would make Be_2ClI a promising candidate material for high-performance radio frequency devices [58].

3 Conclusions

In summary, through a hypothesis-based data-driven approach, we predict a promising family of monolayer MX materials, which hosts Dirac-cone electronic structures at high-symmetry points in the Brillouin zone. With the inclusion of SOC, these materials become quantum spin Hall insulators with sizable band gaps and non-trivial Z_2 topological invariants. VHSs and the corresponding enhanced density of states close in energy to the Dirac point are found for a subclass of the compounds in this family, which offer the potential to host topological superconductivity. We discuss how the Dirac-cone structure

originates through an interplay of the bipartite nature of the hexagonal cation network, incomplete cation-to-anion charge transfer, and the sidewise interactions of the hybridized metal orbitals. Our predicted 2D Dirac materials host high Fermi velocities, which are comparable to that of graphene. The presence of a broad distribution of work functions in the MX 2D materials family would provide opportunities for the realization of novel heterojunction-based devices by taking advantage of the Dirac carriers. Electronic structures of MX monolayers are highly tunable via chemical substitutions and vertical electric field, suggesting the viability of these films for developing platforms for various applications.

Acknowledgements

The authors would like to thank Tay-Rong Chang and Jiatao Sun for helpful discussions. This work was supported by the U.S. Department of Energy, Office of Science, Basic Energy Sciences, under Award #DE-SC0019275. It benefitted from the supercomputing resources of the National Energy Research Scientific Computing Center (NERSC), a U.S. Department of Energy Office of Science User Facility operated under Contract No. DE-AC02-05CH11231, and Temple University's HPC resources supported in part by the National Science Foundation through major research instrumentation grant number 1625061 and by the US Army Research Laboratory under contract number W911NF-16-2-0189. S. X. D. and Y.-F. Z. acknowledge support from the National Key Research and Development Program of China (No. 2016YFA0202300), Strategic Priority Research Program (No. XDB30000000), the National Natural Science Foundation of China (No. 61888102), and the International Partnership Program of the Chinese Academy of Sciences (No. 112111KYSB20160061).

Electronic Supplementary Material: Supplementary material (density functional theory calculation method, carrier mobility, the correlation between work function and cation s orbitals, Fermi velocity, effects of substrate, phonon dispersions, molecular dynamic simulations, crystal orbital Hamiltonian population analysis, electronic and circular polarization in Be_2ClI, and tight-binding analysis) is available in the online version of this article at https://doi.org/10.1007/s12274-020-3022-3.

References

[1] Wang, J. Y.; Deng, S. B.; Liu, Z. F.; Liu, Z. R. The rare two-dimensional materials with Dirac cones. *Natl. Sci. Rev.* **2015**, *2*, 22–39.

[2] Novoselov, K. S.; Geim, A. K.; Morozov, S. V.; Jiang, D.; Zhang, Y.; Dubonos, S. V.; Grigorieva, I. V.; Firsov, A. A. Electric field effect in atomically thin carbon films. *Science* **2004**, *306*, 666–669.

[3] Novoselov, K. S.; Geim, A. K.; Morozov, S. V.; Jiang, D.; Katsnelson, M. I.; Grigorieva, I. V.; Dubonos, S. V.; Firsov, A. A. Two-dimensional gas of massless Dirac fermions in graphene. *Nature* **2005**, *438*, 197–200.

[4] Zhang, Y. B.; Tan, Y. W.; Stormer, H. L.; Kim, P. Experimental observation of the quantum hall effect and Berry's phase in graphene. *Nature* **2005**, *438*, 201–204.

[5] Bolotin, K. I.; Ghahari, F.; Shulman, M. D.; Stormer, H. L.; Kim, P. Observation of the fractional quantum hall effect in graphene. *Nature* **2009**, *462*, 196–199.

[6] Du, X.; Skachko, I.; Duerr, F.; Luican, A.; Andrei, E. Y. Fractional quantum hall effect and insulating phase of Dirac electrons in graphene. *Nature* **2009**, *462*, 192–195.

[7] Dean, C. R.; Wang, L.; Maher, P.; Forsythe, C.; Ghahari, F.; Gao, Y.; Katoch, J.; Ishigami, M.; Moon, P.; Koshino, M. et al. Hofstadter's butterfly and the fractal quantum hall effect in moire superlattices. *Nature* **2013**, *497*, 598–602.

[8] Ponomarenko, L. A.; Gorbachev, R. V.; Yu, G. L.; Elias, D. C.; Jalil, R.; Patel, A. A.; Mishchenko, A.; Mayorov, A. S.; Woods, C. R.; Wallbank, J. R. et al. Cloning of Dirac fermions in graphene superlattices. *Nature* **2013**, *497*, 594–597.

[9] Hunt, B.; Sanchez-Yamagishi, J. D.; Young, A. F.; Yankowitz, M.; LeRoy, B. J.; Watanabe, K.; Taniguchi, T.; Moon, P.; Koshino, M.; Jarillo-Herrero, P. et al. Massive Dirac fermions and hofstadter butterfly in a van der Waals heterostructure. *Science* **2013**, *340*, 1427–1430.

[10] Liu, C. C.; Feng, W. X.; Yao, Y. G. Quantum spin hall effect in silicene and two-dimensional germanium. *Phys. Rev. Lett.* **2011**, *107*, 076802.

[11] Castro Neto, A. H.; Guinea, F.; Peres, N. M. R.; Novoselov, K. S.; Geim, A. K. The electronic properties of graphene. *Rev. Mod. Phys.* **2009**, *81*, 109–162.

[12] Weiss, N. O.; Zhou, H. L.; Liao, L.; Liu, Y.; Jiang, S.; Huang, Y.; Duan, X. F. Graphene: An emerging electronic material. *Adv. Mater.* **2012**, *24*, 5782–5825.

[13] Ashton, M.; Paul, J.; Sinnott, S. B.; Hennig, R. G. Topology-scaling identification of layered solids and stable exfoliated 2D materials. *Phys. Rev. Lett.* **2017**, *118*, 106101.

[14] Mounet, N.; Gibertini, M.; Schwaller, P.; Campi, D.; Merkys, A.; Marrazzo, A.; Sohier, T.; Castelli, I. E.; Cepellotti, A.; Pizzi, G. et al. Two-dimensional materials from high-throughput computational exfoliation of experimentally known compounds. *Nat. Nanotechnol.* **2018**, *13*, 246–252.

[15] Cheon, G.; Duerloo, K. A. N.; Sendek, A. D.; Porter, C.; Chen, Y.; Reed, E. J. Data mining for new two-and one-dimensional weakly bonded solids and lattice-commensurate heterostructures. *Nano Lett.* **2017**, *17*, 1915–1923.

[16] Choudhary, K.; Kalish, I.; Beams, R.; Tavazza, F. High-throughput identification and characterization of two-dimensional materials using density functional theory. *Sci. Rep.* **2017**, *7*, 5179.

[17] Haastrup, S.; Strange, M.; Pandey, M.; Deilmann, T.; Schmidt, P. S.; Hinsche, N. F.; Gjerding, M. N.; Torelli, D.; Larsen, P. M.; Riis-Jensen, A. C. The computational 2D materials database: High-throughput modeling and discovery of atomically thin crystals. *2D Mater.* **2018**, *5*, 042002.

[18] Wallace, P. R. The band theory of graphite. *Phys. Rev.* **1947**, *71*, 622–634.

[19] Cahangirov, S.; Topsakal, M.; Akturk, E.; Şahin, H.; Ciraci, S. Two- and one-dimensional honeycomb structures of silicon and germanium. *Phys. Rev. Lett.* **2009**, *102*, 236804.

[20] Malko, D.; Neiss, C.; Viñes, F.; Görling, A. Competition for graphene: Graphynes with direction-dependent Dirac cones. *Phys. Rev. Lett.* **2012**, *108*, 086804.

[21] Huang, H. Q.; Duan, W. H.; Liu, Z. R. The existence/absence of Dirac cones in graphynes. *New J. Phys.* **2013**, *15*, 023004.

[22] Gomes, K. K.; Mar, W.; Ko, W.; Guinea, F.; Manoharan, H. C. Designer Dirac fermions and topological phases in molecular graphene. *Nature* **2012**, *483*, 306–310.

[23] Vogt, P.; De Padova, P.; Quaresima, C.; Avila, J.; Frantzeskakis, E.; Asensio, M. C.; Resta, A.; Ealet, B.; Le Lay, G. Silicene: Compelling experimental evidence for graphenelike two-dimensional silicon. *Phys. Rev. Lett.* **2012**, *108*, 155501.

[24] Wang, Y. P.; Cheng, H. P. Absence of a Dirac cone in silicene on Ag(111): First-principles density functional calculations with a modified effective band structure technique. *Phys. Rev. B* **2013**, *87*, 245430.

[25] Zhang, L.; Bampoulis, P.; Rudenko, A. N.; Yao, Q.; van Houselt, A.; Poelsema, B.; Katsnelson, M. I.; Zandvliet, H. J. W. Structural and electronic properties of germanene on MoS_2. *Phys. Rev. Lett.* **2016**, *116*, 256804.

[26] Ivanovskii, A. L. Graphynes and graphdyines. *Prog. Solid State Chem.* **2013**, *41*, 1–19.

[27] Hasegawa, Y.; Konno, R.; Nakano, H.; Kohmoto, M. Zero modes of tight-binding electrons on the honeycomb lattice. *Phys. Rev. B* **2006**, *74*, 033413.

[28] Liu, Z. R.; Wang, J. Y.; Li, J. L. Dirac cones in two-dimensional systems: From hexagonal to square lattices. *Phys. Chem. Chem. Phys.* **2013**, *15*, 18855–18862.

[29] Nandkishore, R.; Levitov, L. S.; Chubukov, A. V. Chiral superconductivity from repulsive interactions in doped graphene. *Nat. Phys.* **2012**, *8*, 158–163.
[30] Wu, X. X.; Fink, M.; Hanke, W.; Thomale, R.; Di Sante, D. Unconventional superconductivity in a doped quantum spin Hall insulator. *Phys. Rev. B* **2019**, *100*, 041117.
[31] Jiang, Z.; Henriksen, E. A.; Tung, L. C.; Wang, Y. J.; Schwartz, M. E.; Han, M. Y.; Kim, P.; Stormer, H. L. Infrared spectroscopy of landau levels of graphene. *Phys. Rev. Lett.* **2007**, *98*, 197403.
[32] Ma, F. X.; Jiao, Y. L.; Gao, G. P.; Gu, Y. T.; Bilic, A.; Chen, Z. F.; Du, A. J. Graphene-like two-dimensional ionic boron with double Dirac cones at ambient condition. *Nano Lett.* **2016**, *16*, 3022–3028.
[33] Jiao, Y. L.; Ma, F. X.; Bell, J.; Bilic, A.; Du, A. J. Two-dimensional boron hydride sheets: High stability, massless Dirac fermions, and excellent mechanical properties. *Angew. Chem.* **2016**, *128*, 10448–10451.
[34] Yao, Y. G.; Ye, F.; Qi, X. L.; Zhang, S. C.; Fang, Z. Spin-orbit gap of graphene: First-principles calculations. *Phys. Rev. B* **2007**, *75*, 041401.
[35] Tsai, W. F.; Huang, C. Y.; Chang, T. R.; Lin, H.; Jeng, H. T.; Bansil, A. Gated silicene as a tunable source of nearly 100% spin-polarized electrons. *Nat. Commun.* **2013**, *4*, 1500.
[36] Liu, C. C.; Feng, W. X.; Yao, Y. G. Quantum spin hall effect in silicene and two-dimensional germanium. *Phys. Rev. Lett.* **2011**, *107*, 076802.
[37] Poeppelmeier, K. R.; Corbett, J. D. Metal-metal bonding in reduced scandium halides. Synthesis and crystal structure of scandium monochloride. *Inorg. Chem.* **1977**, *16*, 294–297.
[38] Daake, R. L.; Corbett, J. D. Zirconium monobromide, a second double metal sheet structure. Some physical and chemical properties of the metallic zirconium monochloride and monobromide. *Inorg. Chem.* **1977**, *16*, 2029–2033.
[39] Adolphson, D. G.; Corbett, J. D. Crystal structure of zirconium monochloride. A novel phase containing metal-metal bonded sheets. *Inorg. Chem.* **1976**, *15*, 1820–1823.
[40] Marchiando, J. F.; Harmon, B. N.; Liu, S. H. Electronic structure of layered compounds ZrCl, ZrBr, ScCl and PtTe. *Physica B+C* **1980**, *99*, 259–263.
[41] Wang, B.; Wu, Q. S.; Zhang, Y. H.; Guo, Y. L.; Zhang, X. W.; Zhou, Q. H.; Dong, S.; Wang, J. L. High curie-temperature intrinsic ferromagnetism and hole doping-induced half-metallicity in two-dimensional scandium chlorine monolayers. *Nanoscale Horiz.* **2018**, *3*, 551–555.
[42] Abutalib, M. M. Beryllium chloride monolayer as a direct semiconductor with a tunable band gap: First principles study. *Optik* **2019**, *176*, 579–585.
[43] Park, J. C.; Yun, S. J.; Kim, H.; Park, J. H.; Chae, S. H.; An, S. J.; Kim, J. G.; Kim, S. M.; Kim, K. K.; Lee, Y. H. Phase-engineered synthesis of centimeter-scale 1T′- and 2H-molybdenum ditelluride thin films. *ACS Nano* **2015**, *9*, 6548–6554.
[44] Chang, K.; Hai, X.; Pang, H.; Zhang, H. B.; Shi, L.; Liu, G. G.; Liu, H. M.; Zhao, G. X.; Li, M.; Ye, J. H. Targeted synthesis of 2H- and 1T-phase MoS_2 monolayers for catalytic hydrogen evolution. *Adv. Mater.* **2016**, *28*, 10033–10041.
[45] Deringer, V. L.; Tchougréeff, A. L.; Dronskowski, R. Crystal orbital hamilton population (cohp) analysis as projected from plane-wave basis sets. *J. Phys. Chem. A* **2011**, *115*, 5461–5466.
[46] Wallace, P. R. The band theory of graphite. *Phys. Rev.* **1947**, *71*, 622.
[47] Jiao, Y. L.; Ma, F. X.; Zhang, C. M.; Bell, J.; Sanvito, S.; Du, A. J. First-principles prediction of spin-polarized multiple Dirac rings in manganese fluoride. *Phys. Rev. Lett.* **2017**, *119*, 016403.
[48] Ni, Z. Y.; Liu, Q. H.; Tang, K. C.; Zheng, J. X.; Zhou, J.; Qin, R.; Gao, Z. X.; Yu, D. P.; Lu, J. Tunable bandgap in silicene and germanene. *Nano Lett.* **2012**, *12*, 113–118.
[49] Drummond, N. D.; Zólyomi, V.; Fal'ko, V. I. Electrically tunable band gap in silicene. *Phys. Rev. B* **2012**, *85*, 075423.
[50] Zhang, Y. B.; Tang, T. T.; Girit, C.; Hao, Z.; Martin, M. C.; Zettl, A.; Crommie, M. F.; Shen, Y. R.; Wang, F. Direct observation of a widely tunable bandgap in bilayer graphene. *Nature* **2009**, *459*, 820–823.
[51] Yang, L. M.; Majumdar, K.; Liu, H.; Du, Y. C.; Wu, H.; Hatzistergos, M.; Hung, P. Y.; Tieckelmann, R.; Tsai, W.; Hobbs, C. et al. Chloride molecular doping technique on 2D materials: WS_2 and MoS_2. *Nano Lett.* **2014**, *14*, 6275–6280.
[52] Komsa, H. P.; Kotakoski, J.; Kurasch, S.; Lehtinen, O.; Kaiser, U.; Krasheninnikov, A. V. Two-dimensional transition metal dichalcogenides under electron irradiation: Defect production and doping. *Phys. Rev. Lett.* **2012**, *109*, 035503.
[53] Giovannetti, G.; Khomyakov, P. A.; Brocks, G.; Kelly, P. J.; van den Brink, J. Substrate-induced band gap in graphene on hexagonal boron nitride: *Ab initio* density functional calculations. *Phys. Rev. B* **2007**, *76*, 073103.
[54] Cao, T.; Wang, G.; Han, W. P.; Ye, H. Q.; Zhu, C. R.; Shi, J. R.; Niu, Q.; Tan, P. H.; Wang, E. G.; Liu, B. L. et al. Valley-selective circular dichroism of monolayer molybdenum disulphide. *Nat. Commun.* **2012**, *3*, 887.
[55] Zhang, C. M.; Nie, Y. H.; Sanvito, S.; Du, A. J. First-principles prediction of a room-temperature ferromagnetic Janus VSSe monolayer with piezoelectricity, ferroelasticity, and large valley polarization. *Nano Lett.* **2019**, *19*, 1366–1370.
[56] Bruzzone, S.; Fiori, G. *Ab-initio* simulations of deformation potentials and electron mobility in chemically modified graphene and two-dimensional hexagonal boron-nitride. *Appl. Phys. Lett.* **2011**, *99*, 222108.
[57] Qiao, J. S.; Kong, X. H.; Hu, Z. X.; Yang, F.; Ji, W. High-mobility transport anisotropy and linear dichroism in few-layer black phosphorus. *Nat. Commun.* **2014**, *5*, 4475.
[58] Schwierz, F.; Pezoldt, J.; Granzner, R. Two-dimensional materials and their prospects in transistor electronics. *Nanoscale* **2015**, *7*, 8261–8283.